TECHNICAL PAPER

CrossMark

The piezoresistance of a device with polyphenylenevinylene derivative PSS-PPV film

Jie Li[1] · Yu-xuan Hou[1] · Yu-yan Wang[1] · Fei Ye[1] · Gao-yu Zhong[1]

The mechanical and electrical characteristics of poly[1-methoxy-4-(3-propyloxy-heptaisobutyl-PSS)-2,5-phenylenevinylene] (PSS-PPV) film were studied in this work. The loading curves and Young's modulus of PSS-PPV film were measured with nanoindentation tests. The device ITO/PSS-PPV (75 nm)/Al (100 nm) was fabricated and measured to obtain the current–voltage (I–V) and current-time (I–T) curves under different pressures ranging in 0–163 kPa. The device demonstrated high sensitivity, good stability, and nice repeatability. The piezoresistance coefficient can even reach 2.0×10^{-3} Pa^{-1} at 0.2 V and 111 kPa. The time and charges required to form a stable build-in electric field in the device under different pressures were analyzed using a high-frequency square-wave voltage. It is deduced that the applied pressure not only tightens the PSS-PPV film but also improves its conductance. This property makes PSS-PPV film possess prospect in pressure sensing applications, though it still suffers from partly slow recovering after considerable compression.

1 Introduction

Organic conjugated polymers are very attractive in the sensitive materials due to their good piezoresistive characteristics, mechanical flexibility and easy processing (Zhao et al. 2017; Li et al. 2016; Kim et al. 2011a, b; Jiang and Cao 2010; Zhong et al. 2009; Dong et al. 2006), which can meet the sophisticated technical demands in the field of artificial intelligence, such as robotic electronic skins (Hammock et al. 2013; Ilievski et al. 2011; Mascaro and Asada 2004) and minimally invasive surgery (Kim et al. 2011a, b). There are mainly four kinds of piezoresistive materials used in tactile sensors (Amjadi et al. 2016; Stassi et al. 2014; Maheshwari and Saraf 2008): (1) metal in strain gauges (Maheshwari and Saraf 2008; Graz et al. 2009; Amjadi et al. 2014; Deng et al. 2018); (2) inorganic semiconductors (Kanda 1982; Barlian et al. 2009; Cotton et al. 2009); (3) conductive polymer composites (Wichmann et al. 2009; Tee et al. 2012; Sanli et al. 2017), e.g., the composite of carbon particle filled polydimethylsiloxane (PDMS); (4) organic conjugated polymers (Tahk et al. 2009; Li et al. 2014; Nunes Pereira et al. 2012; Wang et al.

2016). Among these materials, conductive polymer composites have been widely investigated and used for many years (Wichmann et al. 2009; Tee et al. 2012). Although the composite material has many advantages, an intractable problem is that, as a physical hybrid, the phase segregation will affect the device performance (Lipomi et al. 2011). Recently, many conjugated polymers show prospects in tactile sensors due to their excellent performances, such as flexibility, high sensitivity, low cost, lightness and thin thickness (Tahk et al. 2009; Choong et al. 2014; Li et al. 2005; Wang et al. 2016). These pressure sensitive characteristics can generally attribute to the molecular structure with good conductive conjugated main chains and insulated flexible side chains (Braun and Heeger 1991; Chandrasekhar et al. 2001). The intermolecular space will decrease and the overlap of molecular orbitals will increase if the film is compressed, which increases the probability of electron transfer between molecules. Thus the conductivity of materials will increase with the increasing pressures. The PPV derivatives, as one kind of conjugated polymers, have been extensively studied for their potential applications in display and tactile sensors (Malliaras et al. 1998; Zhong et al. 2009; Dai et al. 2013; Hou et al. 2017). The branch chains in these PPV derivatives are usually alkyls. Extending the branch alkyl chain will soften the polymer and reduce its conductance. However, the polymer will become hard to recover the

✉ Gao-yu Zhong
  gyzhong@fudan.edu.cn

[1] Department of Materials Science, Fudan University, Shanghai 200433, China

original shape when it is compressed to a degree if the branch chain is too long (e.g., the branch chain has twelve carbons) (Song et al. 2017). This is due to the high viscoelasticity of the branch alkyl chain.

The piezoresistance studies on PPV derivatives with alkyl as the branch chain show that the sensitive pressure normally ranged in 0–300 or 0–500 kPa (Zhong et al. 2009; Hou et al. 2017). Mascaro and Asada (2004) reported that the tactile sense of human hands usually ranged from 10 to 40 kPa (Maheshwari and Saraf 2006, Maheshwari and Saraf 2008). So we have to improve the sensitivity of the piezoresistive materials to make the sensing material softer and more suitable for working in low pressures. The reason why PSS-PPV can be selected as the sensing material mainly due to the big volume of the cage-like branch, polyhedral oligomeric silsesquioxane (POSS), which enlarged the intermolecular space between the conductive PPV main chains. A little stress may produce a big deformation, leading to a significant change in resistance and making the material more sensitive.

In the present work, we fabricated device ITO/PSS-PPV/Al which worked in the range of 0–163 kPa. The piezoresistance coefficient ranged in $(1.86–20.0) \times 10^{-4}$ Pa^{-1}. When the pressure is 111 kPa and the voltage is 0.2 V, the piezoresistance coefficient reached the maximum 2.0×10^{-3} Pa^{-1}. We measured the current in the device under different stresses with a high-frequency (2.5 kHz) square-wave voltage. The time and charges required to form a stable build-in electric field under different pressures were analyzed. Both tendencies of time and charges varying with pressure are consistent with each other. It can be concluded that the applied pressure tightened the PSS-PPV film, which led a faster formation of a stable electric field and lessened the required charges in this field formation. However, the delay time of the slow process of the film rebounding was simulated to be ~ 550 s by using the Voigt–Kelvin parallel model, which means the material needs a long time to recover completely from a normal compression.

2 Experimental details

The PSS-PPV used in this study is bought from Sigma-Aldrich company (http://www.sigmaaldrich.com). The molecular structure is shown in Fig. 1. The Young's modulus and loading curves of the organic conjugated polymers were measured with a nanoindentation tester (CSM, Switzerland, UNHT) using the Oliver and Pharr method (Doerner and Nix 1986; Oliver and Pharr 1992; Cao et al. 2007a). The chloroform solution (5 mg/ml) of PSS-PPV was dropped onto a clean silicon wafer and dried in air to obtain a PSS-PPV film for nanoindentation test.
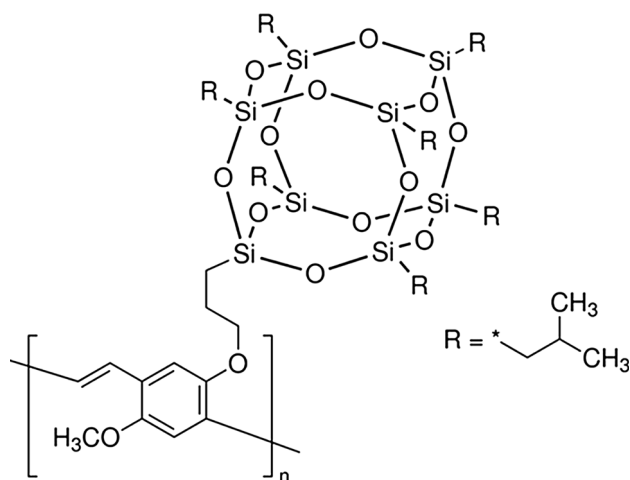

Fig. 1 The molecular structure of PSS-PPV

The thickness of the film was measured with a surface profilometer (BRUKER DEKTAK150). In order to prevent damaging the film surface during the loading process, we used a diamond cylinder with 20 μm diameter as the flat punch. The initial load is 0.03 mN and the maximum load is 0.1 mN. The loading/unloading rate is 0.1 mN/min. The dwell time between the loading and unloading process is 20 s. Eight cycles of loading/unloading processes were carried out in this multicycle test.

We fabricated the devices on cleaned ITO patterned glass substrates. The device structure is shown in Fig. 2. The ITO glass was cleaned by ultrasonic cleaning with acetone, ethanol and deionized water for 5 min, respectively. PSS-PPV was dissolved in chloroform (5 mg/ml) and then the solution was spin-coated on the ITO glass at 1000 r/min rate for 60 s. After drying, a 100-nm-thick Al film was evaporated on the surface of the PSS-PPV film. Finally, we obtained the piezoresistive device ITO/PSS-PPV (75 nm)/Al (100 nm) with an active area of 3×3 mm^2. We used Digital Force Gauge (AIPU, HF-1) to apply different pressures on the device and digital source

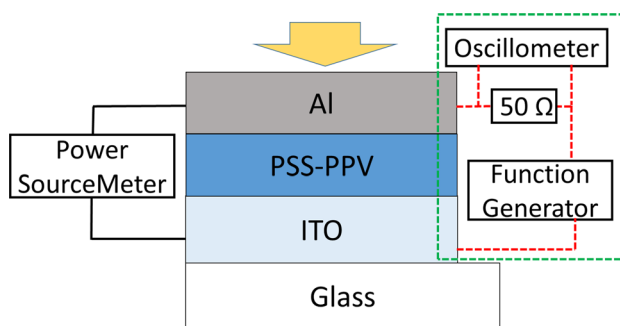**Fig. 2** Device structure and test mode. In the green dashed line frame, the oscilloscope is used to measure the transient voltage at the 50 Ω resistance of the series connected in the circuit to test the time-dependent current under the high-frequency square-wave voltage

meter (Keithley, 2400) as the power supply to test the electrical characteristics. The current-voltage (I–V) and current-time (I–T) curves under different pressures were obtained. We put a silicon wafer (3×3 mm^2) on the device to make the polished surface fully contact the device active area, and the pressure was applied at the wafer's center to ensure that the pressure was applied smoothly and distributed uniformly on the active area.

We applied the high-frequency square-wave voltage (2.5 kHz) on the device with a function generator. The low and high levels are -3 and 3 V, respectively. A 50-Ω resistor was connected in series with the circuit. The voltage on this resistor was measured with an oscilloscope (Tektronix-AFG2021 model). We obtained the time-dependent voltage and current under different pressures. We calculated the time and charges required in the formation of a stable built-in electric field with different pressures, trying to understand the piezoresistive mechanisms.

3 Results and discussion

We measured the mechanical properties of the PSS-PPV film using multicycle test, obtained the loading curves as shown in Fig. 3. The thickness of the film is about 7.1 μm, roughness is 5.2 nm, and the average Young's modulus is 45 MPa. This Young's modulus is much more lower than those of other PPV derivatives (Zhong et al. 2009; Hou et al. 2017), but is higher than that of a normal PDMS, which is ~ 1 MPa for the PDMS with two-component Sylgard 184 silicone kit (S184) from Dow Corning mixed in the weight ratio of 10:1 (O'Connor et al. 2010). We suppose that the low modulus of PSS-PPV is due to the elastic properties of the cage-like POSS group in this molecule, which is similar to the –Si–O–

bonds in PDMS, making the material incompact and easier to be compressed.

Figure 3a shows that the creep occurred within the dwell time (20 s) under the maximum force (0.1 mN). The first compression on the pristine film exhibited the most serious creep. Then the creep decreased gradually with the test cycles. The loading curves show that the eighth cycle test even repeated the seventh, indicating that the space between polymer molecules is almost removed by the pressure. Then the film became elastic and exhibited a good repeatability under the ordinary compressing stress. Figure 3b shows that the indented depth (deformation) is normally greater than the rebounded depth during the cyclic loading/unloading processes, which indicates that the rebounding of material is far slower than the compression. More evidence will be discussed in the following analysis.

We measured the current-voltage (I–V) characteristics of the device ITO/PSS-PPV/Al under different pressures. As shown in Fig. 4, it indicates that the external pressure reduces the device resistance obviously. At the same voltage, the current density increased along with the increasing pressures and it is close to saturation when the pressure is about 150 kPa. The device demonstrates a good piezoresistive performance in the range of 0–150 kPa.

The current density varying with pressure (J–P curve) at different voltages is shown in Fig. 5. It is obvious that the current density increases with the applied pressure at different voltages until the current tends to saturate at ~ 150 kPa. It can be also used for analyzing the piezoresistive characteristics of this device.

Figure 6a shows that the enlargement factors of the current gradually decreases with the voltage under different pressures. That implies the device normally has a relative higher enlargement factor at low voltages and a bigger
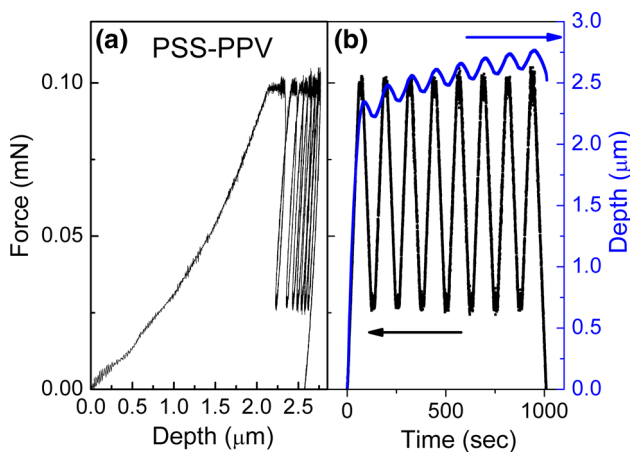

Fig. 3 The loading-unloading curve measured in a multicycle test (**a**); the indented depth and the load varying with time (**b**)
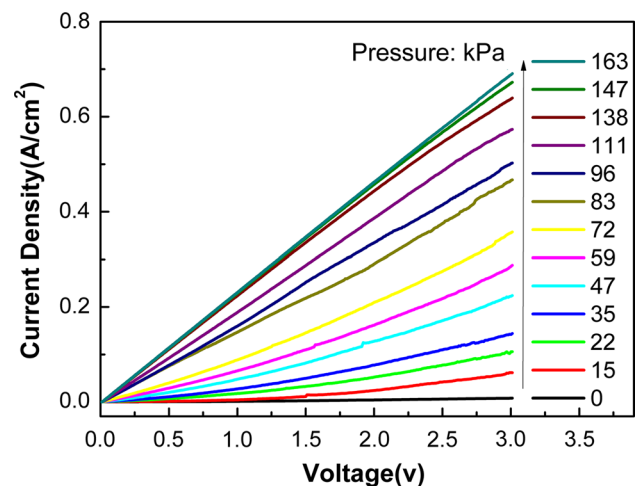

Fig. 4 The J–V curve under different pressures ranging in 0–163 kPa

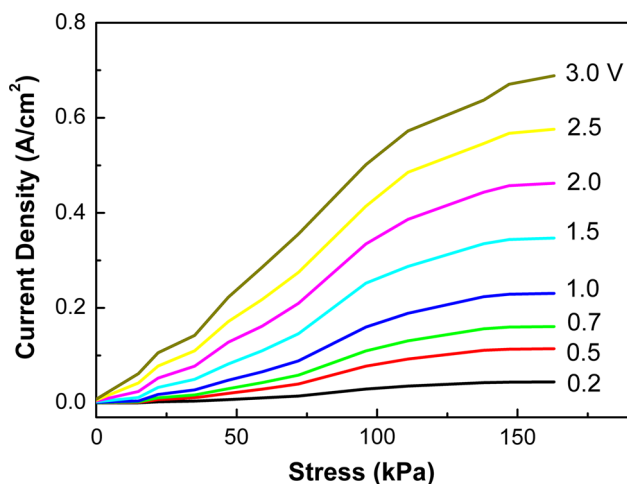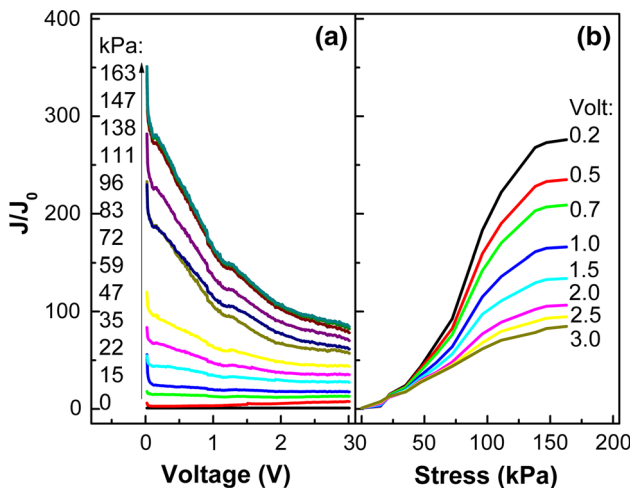**Fig. 5** The current density varying with stress under different voltages

Fig. 6 The current enlargement factors with the voltage under different pressures (**a**); the current enlargement factors with the pressure under different voltages (**b**)

current variation at high voltages. So the device working voltage can be very low and thus the energy consumption is also low. As shown in Fig. 6b, we can find that the current increases 275 times at 0.2 V and 140 kPa, indicating that the current changes significantly with the applied pressure.

The piezoresistance coefficient can describe the sensitivity of a piezoresistive device, which implies the ability of a device responding to external pressure (He and Yang 2006). Researchers define the relative change of the electrical conductivity caused by the unit pressure as the piezoresistance coefficient π_l^p (Milne et al. 2010):

$$\pi_l^p = \frac{1}{P}\frac{\Delta\sigma}{\sigma_0} = \frac{1}{P}\frac{\Delta J}{J_0}, \tag{1}$$

where σ_0 and $\Delta\sigma$ represent the initial conductivity and its variation of the device, respectively. J_0 and ΔJ represent the

initial current density and its variation, respectively. P is the external pressure. Figure 7 shows the piezoresistance coefficient of the device changing with pressure at different voltages. It is obvious that the piezoresistance coefficient increases significantly with the increasing pressure in the range of 0–111 kPa. However, the piezoresistance coefficient decreases slowly with the increasing pressure when the pressure is higher than 111 kPa. The piezoresistance coefficient ranges in $(1.86–20.0) \times 10^{-4}$ Pa^{-1}. When the pressure is 111 kPa and the voltage is 0.2 V, the piezoresistance coefficient of the device reaches the maximum 2.0×10^{-3} Pa^{-1}, about five orders of magnitude higher than the piezoresistance coefficient of inorganic silicon pressure sensor (Cao et al. 2007b). The pressure felt by human fingers is generally considered to range from 10 to 40 kPa (Maheshwari and Saraf 2006). In this range, the piezoresistance coefficient of PSS-PPV device roughly ranged in $(1.86–9.28) \times 10^{-4}$ Pa^{-1}. So the PSS-PPV device has a high sensitivity.

We measured the current of the device at 3 V under different pressures in order to study the stability of the piezoresistive performance. Figure 8a shows that the current is stable under a fixed pressure. For investigating the sensitivity and repeatability of the device, we applied square-wave voltage on the device which is shown at the bottom of Fig. 8b. The low and high levels of the voltages are 0 and 3 V, respectively. The duration of the low and high levels are 10 s. We set the high level to be 3 V instead of 0.2 V, mainly because of the big current and its variation. The high sensitivity of current to pressure leads the current fluctuates seriously during the pressure changing process. So we changed the pressure in the duration of 0 V low level to prevent the current fluctuation, as shown in Fig. 8b. The device shows a quick response and a good repeatability in the sensing process.
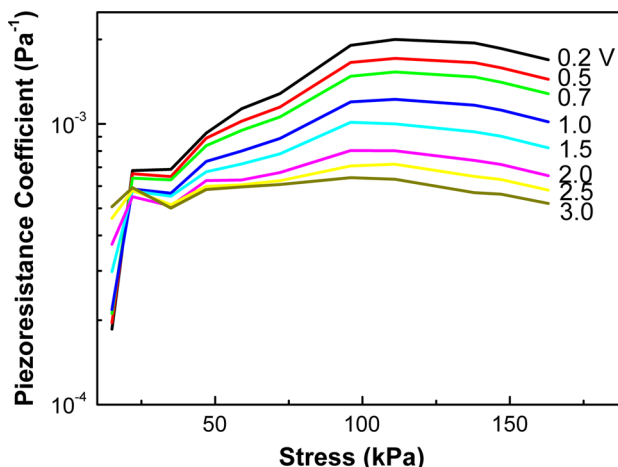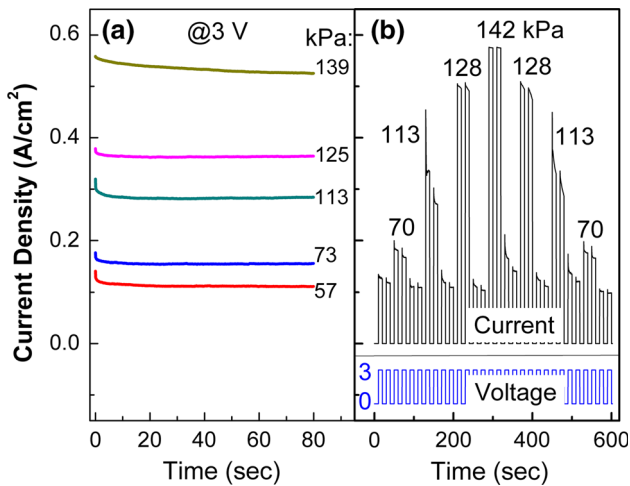

Fig. 7 The piezoresistance coefficient with the increasing stress in the range of 0–163 kPa under different voltages

Fig. 8 The time-dependent current density under different pressures at 3 V voltage (**a**); the time-dependent current density with the varying pressures under a square-wave voltage applied on the device (**b**). The low and high levels of the voltages are 0 and 3 V, respectively. The duration of the low or high level is 10 s

We applied 0 and 150 kPa alternatively and 3 V constant voltage on the device. The current varying with time is shown in Fig. 9a. We found that the current increased very fast when the pressure loaded. However, the current decreased more slowly when the pressure unloaded. It can be seen that when the pressure increases rapidly from 0 to 150 kPa, the current also increases rapidly, which indicates that the device responses fast to pressure. The current measured with the same force is basically consistent, confirming the good repeatability and reliability of the device. However, Fig. 9a shows that, when the pressure dropped from 150 to 0 kPa, the current decreased quickly at first (within one second), and then continued to decrease
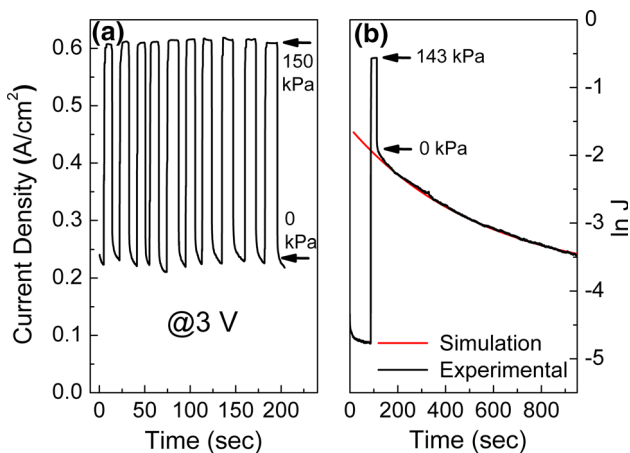
Fig. 9 The time-dependent current density with alternative 0 and 150 kPa and 3 V constant voltage applied on the device (**a**). The time-dependent current density with a 143 kPa stress applied on the device for 23 seconds and then the stress was removed (**b**)

slowly in the next 20 s. The gradually decreasing process looks lasting for a long period.

As shown in Fig. 9b, we carried out a test with a longer duration to study the slow response when the pressure is removed. We applied a pressure (143 kPa) on the device and kept the current stable for 23 s, then the pressure was removed. We found that the current decreased with a fast process and a slow process. The fast process lasted for less than 1 s, while the slow process lasted for a period longer than 840 s. We think that the fast process related to the resilience of the elastic part of the PSS-PPV film, while the slow process may relate to the slow resilience of the cage-like POSS branches in the PSS-PPV molecules. The POSS consists of many –Si–O– bonds. Its large volume makes itself loose and deforms easily, exhibiting a soft characteristic and a slow rebounding from deformation. It shows that the PSS-PPV film is viscoelastic and difficult to recover the deformation rapidly and completely when the external pressure is removed. Thus the device current decreased slowly with the slow complete recovering of the PSS-PPV film deformation.

We can deduce that the creep occurred through the phenomenon that the strain increases with time when a constant stress is kept on a solid material (Cheng et al. 2000; Tweedie and Van Vliet 2006). The Voigt–Kelvin parallel model is a simple classic model which describes the mechanism of creep. The differential equation about stress and strain is (FURUKAWA et al. 1984; Schuetrumpf et al. 2012):

$$\sigma(t) = G\varepsilon + \eta \frac{d\varepsilon}{dt}, \tag{2}$$

where G is the modulus, η is the viscosity, ε is the strain, and σ is the stress applied on the material. If we remove the external stress, the model can also describe the stress-strain relationship during the slow recovering process.

At the initial stable state, we can know from formula (2) that $t = 0$, $\frac{d\varepsilon}{dt} = 0$, and. $\sigma(0) = G\varepsilon_0$. When the pressure is removed ($\sigma = 0$), Eq. (2) should be:

$$\eta \frac{d\varepsilon}{dt} + G\varepsilon = 0. \tag{3}$$

So the time-dependent strain should be:

$$\varepsilon(t) = \varepsilon_0 \cdot e^{-\frac{t}{\tau}}, \tag{4}$$

where $\tau = \eta/G$, the τ is delay time, indicating the degree of slow response of strain onto stress and describing the viscous behavior of materials. A greater delay time represents that a longer period is needed for the strain recovery.

The relationship between current density and strain can be described by the equation below (see Eq. 17 and fig. 6 in reference Dai et al. 2013):
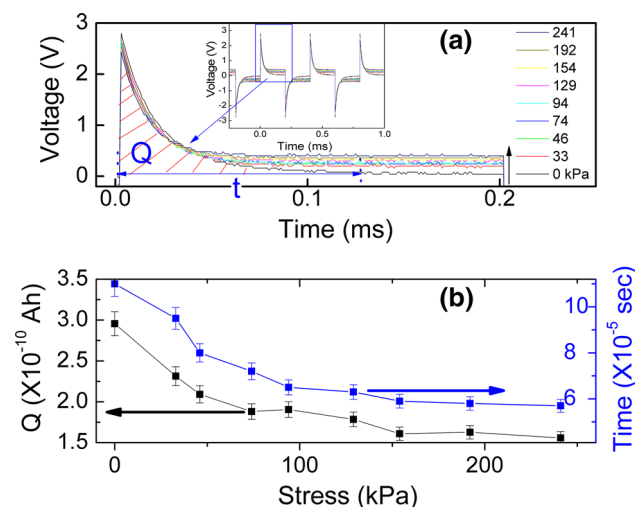
Fig. 10 The time-dependent voltage measured with an oscilloscope on a 50 Ω resistor which connected in series into the circuit (**a**); the continuous 2.5 kHz square-wave voltage was produced with a function generator; the required quantity of electric charge and the time needed in the device to establish a stable electric field varying with the applied pressures (**b**)

$$\ln\frac{j(\varepsilon_t)}{j(0)} = \frac{\varepsilon_t}{k}, \tag{5}$$

where k represents the slope of the loading curve. So we can combine the Eq. (4) with Eq. (5), then obtained Eq. (6) :

$$\ln j(\varepsilon_t) = \frac{\varepsilon_0}{k} e^{-\frac{t}{\tau}} + \ln j(0). \tag{6}$$

We use Eq. (6) to fit the time-dependent current in Fig. 9b, then obtained:

$$\ln j(\varepsilon_t) = 2.25 e^{-\frac{t}{550}} - 3.85. \tag{7}$$

So the delay time is 550 s. It indicates that the device shows a little slow on full recovery if the considerable compression (143 kPa) is suddenly removed as the applied high voltage (3 V) keeps on it.

We applied 2.5 kHz square-wave voltage on the device to investigate the electrical stabilizing process. The circuit is shown in the dotted line box in Fig. 2. We used a function generator to output a continuous square-wave voltage and applied on the device. We used an oscilloscope to measure the voltage on the 50 Ω resistor which was connected in series with the circuit. The time-dependent voltage is directly proportional to the device current, which is shown in the inset of Fig. 10a. We found that the stabilized voltage on the 50 Ω resistor increased along with the increasing stress, indicating that the stabilized current increases and the device resistance decreases with the increasing pressure.

We studied one of these cycles. As shown in Fig. 10a, the device current decreased with the elapsing time at first

and then reach a constant, indicating that the device needs a period to form a stable built-in electric field. It can be seen that this period becomes shorter if the pressure increases. The trapped charges have been analyzed with the time integration of current during this current stabilization period, which also shows the charge quantity required in the establishment of a stable built-in electric field. We calculated these charge quantities from the time-dependent voltage on the 50 Ω resistor. The quantity of electric charge and the time required in the device to establish a stable electric field under different pressures are shown in Fig. 10b. The required time and charges decrease obviously with the increasing stress when the device is pressed, which means that the stress lessens carrier traps, making carriers escape from traps more easily. The applied pressure makes the PSS-PPV film tighter, more conductive, filling fewer carrier traps, and faster forming of a stable built-in electric field.

4 Conclusions

In summary, Young's modulus of PSS-PPV film is measured with nanoindentation to be about 45 MPa. The device ITO/PSS-PPV/Al is fabricated and measured to obtain the I–V and I–T characteristics under different pressures. The piezoresistance coefficient of this device is measured to be $(1.86–20.0) \times 10^{-4}$ Pa^{-1}. The device achieves the maximum piezoresistive coefficient 2.0×10^{-3} Pa^{-1} at 111 kPa pressure and 0.2 V working voltage. The working pressure ranges from 0 to 150 kPa approximately. Further tests show that the device has good repeatability, stability, and sensitivity. The applied pressure enhances the conductivity of PSS-PPV device. We also found that the time and charges required to form a stable build-in electric field in the device decreased with the increasing pressures.

References

Amjadi M, Pichitpajongkit A, Lee S, Ryu S, Park I (2014) Highly stretchable and sensitive strain sensor based on silver nanowire–elastomer nanocomposite. ACS Nano 8(5):5154–5163

Amjadi M, Kyung K, Park I, Sitti M (2016) Stretchable, skin-mountable, and wearable strain sensors and their potential applications: a review. Adv Funct Mater 26(11):1678–1698

Barlian AA, Park WT, Mallon JR, Rastegar AJ, Pruitt BL (2009) Review: semiconductor piezoresistance for microsystems. Proc IEEE 97(3):513–552

Braun D, Heeger AJ (1991) Visible-light emission from semiconducting polymer diodes. Appl Phys Lett 58(18):1982–1984

Cao JX, Gong XG, Wu RQ (2007a) Giant piezoresistance and its origin in Si(111) nanowires: first-principles calculations. Phys Rev B 75(23):233302

Cao YP, Dao M, Lu J (2007b) A precise correcting method for the study of the superhard material using nanoindentation tests. J Mater Res 22(5):1255–1264

Chandrasekhar M, Guha S, Graupner W (2001) Squeezing organic conjugated molecules—what does one learn? Adv Mater 13(8):613

Cheng L, Xia X, Yu W, Scriven LE, Gerberich WW (2000) Flat-punch indentation of viscoelastic material. J Polym Sci Polym Phys 38(1):10–22

Choong C, Shim M, Lee B, Jeon S, Ko D, Kang T, Bae J, Lee SH, Byun K, Im J, Jeong YJ, Park CE, Park J, Chung U (2014) Highly stretchable resistive pressure sensors using a conductive elastomeric composite on a micropyramid array. Adv Mater 26(21):3451–3458

Cotton DPJ, Graz IM, Lacour SP (2009) A multifunctional capacitive sensor for stretchable electronic skins. IEEE Sens J 9(12):2008–2009

Dai W, Zhang B, Kang Y, Chen H, Zhong G, Li Y (2013) The stress-affected carrier injection and transport in organic semiconductor devices. J Phys D Appl Phys 46:38510338

Deng C, Pan L, Li C, Fu X, Cui R, Nasir H (2018) Helical gold nanotube film as stretchable micro/nanoscale strain sensor. J Mater Sci 53(3):2181–2192

Doerner MF, Nix WD (1986) A method for interpreting the data from depth-sensing indentation instruments. J Mater Res 1(4):601–609

Dong B, Lu N, Zelsmann M, Kehagias N, Fuchs H, Sotomayor Torres CM, Chi LF (2006) Fabrication of high-density, large-area conducting-polymer nanostructures. Adv Funct Mater 16(15):1937–1942

Furukawa T, Date M, Ohuchi M, Chiba A (1984) Ferroelectric switching characteristics in a copolymer of vinylidene fluoride and trifluorethylene. J Appl Phys 56(5):1481–1486

Graz IM, Cotton DPJ, Lacour SP (2009) Extended cyclic uniaxial loading of stretchable gold thin-films on elastomeric substrates. Appl Phys Lett 94:0719027

Hammock ML, Chortos A, Tee BCK, Tok JBH, Bao Z (2013) 25th Anniversary Article: the evolution of electronic skin (e-skin): a brief history, design considerations, and recent progress. Adv Mater 25(42):5997–6038

He R, Yang P (2006) Giant piezoresistance effect in silicon nanowires. Nat Nanotechnol 1(1):42–46

Hou W, Gao L, Tian Y, Yan W, Hou Y, Li J, Zhong G (2017) Stress-induced variation of MDMO-PPV film thickness and resistance. Synth Met 226:113–118

Ilievski F, Mazzeo AD, Shepherd RF, Chen X, Whitesides GM (2011) Soft robotics for chemists. Angew Chem Int Ed 50(8):1890–1895

Jiang ZY, Cao XA (2010) Stress-induced current and luminescence modulations in an organic light-emitting device. Appl Phys Lett 97(20):203304

Kanda Y (1982) A graphical representation of the piezoresistance coefficients in silicon. IEEE Trans Electron Dev 29(1):64–70

Kim BY, Rutka JT, Chan WC (2011a) Nanomedicine. N Engl J Med 363(25):2434–2443

Kim FS, Ren G, Jenekhe SA (2011b) One-dimensional nanostructures of π-conjugated molecular systems: assembly, properties, and applications from photovoltaics, sensors, and nanophotonics to nanoelectronics. Chem Mater 23(3):682–732

Li Y, Cheng XY, Leung MY, Tsang J, Tao XM, Yuen MCW (2005) A flexible strain sensor from polypyrrole-coated fabrics. Synth Met 155(1):89–94

Li M, Li H, Zhong W, Zhao Q, Wang D (2014) Stretchable conductive polypyrrole/polyurethane (PPy/PU) strain sensor with netlike microcracks for human breath detection. ACS Appl Mater Interfaces 6(2):1313–1319

Li Z, Ma G, Ge R, Qin F, Dong X, Meng W, Liu T, Tong J, Jiang F, Zhou Y, Li K, Min X, Huo K, Zhou Y (2016) Free-standing conducting polymer films for high-performance energy devices. Angew Chem Int Ed 55(3):979–982

Lipomi DJ, Vosgueritchian M, Tee BC, Hellstrom SL, Lee JA, Fox CH, Bao Z (2011) Skin-like pressure and strain sensors based on transparent elastic films of carbon nanotubes. Nat Nanotechnol 6(12):788–792

Maheshwari V, Saraf RF (2006) High-resolution thin-film device to sense texture by touch. Science 312(5779):1501–1504

Maheshwari V, Saraf R (2008) Tactile devices to sense touch on a par with a human finger. Angew Chem Int Ed 47(41):7808–7826

Malliaras GG, Salem JR, Brock PJ, Scott C (1998) Electrical characteristics and efficiency of single-layer organic light-emitting diodes. Phys Rev B 58(20):13411–13414

Mascaro SA, Asada HH (2004) Measurement of finger posture and three-axis fingertip touch force using fingernail sensors. IEEE Trans Robot Autom 20(1):26–35

Milne JS, Rowe ACH, Arscott S, Renner C (2010) Giant piezoresistance effects in silicon nanowires and microwires. Phys Rev Lett 105:22680222

Nunes Pereira J, Vieira P, Ferreira A, Paleo AJ, Rocha JG, Lanceros-Mendez S (2012) Piezoresistive effect in spin-coated polyaniline thin films. J Polym Res 19:98152

O'Connor B, Chan EP, Chan C, Conrad BR, Richter LJ, Kline RJ, Heeney M, McCulloch I, Soles CL, DeLongchamp DM (2010) Correlations between mechanical and electrical properties of polythiophenes. ACS Nano 4(12):7538–7544

Oliver WC, Pharr GM (1992) An improved technique for determining hardness and elastic-modulus using load and displacement sensing indentation experiments. J Mater Res 7(6):1564–1583

Sanli A, Benchirouf A, Mueller C, Kanoun O (2017) Piezoresistive performance characterization of strain sensitive multi-walled carbon nanotube-epoxy nanocomposites. Sens Actuators A Phys 254:61–68

Schuetrumpf J, Zhukov S, Genenko YA, von Seggern H (2012) Polarization switching dynamics by inhomogeneous field mechanism in ferroelectric polymers. J Phys D Appl Phys 45:16530116

Song Y, Chen H, Su Z, Chen X, Miao L (2017) Highly compressible integrated supercapacitor-piezoresistance-sensor system with CNT-PDMS sponge for health monitoring. Small 13:1702091

Stassi S, Cauda V, Canavese G, Pirri C (2014) Flexible tactile sensing based on piezoresistive composites: a review. Sensors Basel 14(3):5296–5332

Tahk D, Lee HH, Khang D (2009) Elastic moduli of organic electronic materials by the buckling method. Macromolecules 42(18):7079–7083

Tee BC, Wang C, Allen R, Bao Z (2012) An electrically and mechanically self-healing composite with pressure- and flexion-sensitive properties for electronic skin applications. Nat Nanotechnol 7(12):825–832

Tweedie CA, Van Vliet KJ (2006) Contact creep compliance of viscoelastic materials via nanoindentation. J Mater Res 21(6):1576–1589

Wang J, Karmakar RS, Lu Y, Wu M, Wei K (2016) Nitrogen plasma surface modification of Poly(3,4-ethylenedioxythiophene):poly(styrenesulfonate) films to enhance the piezoresistive pressure-sensing properties. J Phys Chem C 120(45):25977–25984

Wichmann MHG, Buschhorn ST, Gehrmann J, Schulte K (2009) Piezoresistive response of epoxy composites with carbon nanoparticles under tensile load. Phys Rev B 80:24543724

Zhao S, Li J, Cao D, Zhang G, Li J, Li K, Yang Y, Wang W, Jin Y, Sun R, Wong C (2017) Recent advancements in flexible and stretchable electrodes for electromechanical sensors: strategies, materials, and features. ACS Appl Mater Int 9(14):12147–12164

Zhong GY, Zhang YQ, Cao XA (2009) Conjugated polymer films for piezoresistive stress sensing. IEEE Electr Device Lett 30(11):1137–1139